Heat-Induced Stretching of a Glass Tube Under Tension: Applications to Glass Microelectrodes

Huaxiong Huang[1], Robert M. Miura[2,3,4], William P. Ireland[5], and Ernest Puil[4]

[1] Department of Mathematics and Statistics
York University, Toronto, ON Canada M3J 1P3

[2] Departments of Mathematical Sciences and
Biomedical Engineering and
Center for Applied Mathematics and Statistics
New Jersey Institute of Technology, Newark, NJ 07102 USA

[3] Department of Mathematics and
Institute of Mathematical Sciences
University of British Columbia, Vancouver, BC Canada V6T 1Z2

[4] Department of Pharmacology and Therapeutics
University of British Columbia, Vancouver, BC Canada V6T 1Z3

[5] Department of Anatomy and Physiology
University of Prince Edward Island
Charlottetown, PE Canada C1A 4P3

CAMS Report 0203-26, Spring 2003

Center for Applied Mathematics and Statistics

NJIT

HEAT-INDUCED STRETCHING OF A GLASS TUBE UNDER TENSION: APPLICATION TO GLASS MICROELECTRODES

Huaxiong Huang[1], Robert M. Miura[2,3,4], William P. Ireland[5], and Ernest Puil[3]

[1] Department of Mathematics and Statistics, York University, Toronto, Ontario, Canada M3J 1P3.
[2] Department of Mathematics and Institute of Applied Mathematics, University of British Columbia, Vancouver, B.C., Canada V6T 1Z2.
[3] Department of Pharmacology & Therapeutics, University of British Columbia, Vancouver, B.C., Canada V6T 1Z3.
[4] Department of Mathematical Sciences, New Jersey Institute of Technology, Newark, N.J. 07102, USA.
[5] Department of Anatomy and Physiology, University of Prince Edward Island, Charlottetown, P.E.I., Canada C1A 4P3.

Abstract

Deformation of glass using heat occurs in many industrial and artistic applications, including the manufacturing of laboratory glass products, drawing of fiber optics, and hand-blown artistic creations. The formation of glass objects is an art, but the trial-and-error procedures can be reduced by development of a systematic theory, especially when the objects are formed using mechanical means. Glass microelectrodes are ubiquitous in experimental studies of the electrophysiology of biological cells and their membranes, and the "pulling" of these electrodes is based on trial-and-error. To make this process more systematic, we derive a model for glass microelectrode formation using a coil heater with a gravity-forced electrode puller assuming the glass tube is an incompressible, viscous fluid. The model is one dimensional, and the effects of thermal radiation from the coil heater are essential in the formation process. A breaking stress criterion is imposed to fracture the glass tube, forming the electrode tip. The difficulty with the moving free end is avoided by introducing a quasi-Lagrangian coordinate system. The model equations are solved using an adaptive moving grid to account for the local stretching of the glass. A number of examples using a double-pull paradigm have been computed to illustrate the dependence of the electrode shape and tip diameter on the heater temperature and the ratio between the inner and outer radii.

1 Introduction

Glass objects routinely are produced in industry and in some technical arts. Such objects include laboratory products, fiber optics, and hand-blown glassware. In some applications,

heat is applied to soften the glass during the formation of these glass objects, using trial-and-error procedures. However, when these procedures involve mechanical devices, the use of mathematical models provides a more systematic approach. For example, the pulling of glass fiber optics has been studied by Fitt et al. ([1]) and other researchers ([4, 12]). Most of these studies focus on isothermal or prescibed temperature conditions, and given pulling velocities.

Glass microelectrodes have played an essential role in cell electrophysiology for decades and will continue to be an important tool in the future. These micropipettes are used to inject electric current and dyes into cells and measure membrane potentials by inserting them through cellular membranes or to form a patch clamp of the membrane. The data collected give information of membrane electrical properties in the presence of voltage-gated and receptor-gated ion channels and with the application of drugs. Laboratories using these microelectrodes usually make them on a daily basis using commercially available glass tubes and electrode pullers that use coil heaters for softening the glass tubes during the stretching procedure.

There are four experimentally relevant parameters that can be measured on glass microelectrodes. They are tip length, tip diameter, electrode resistance, and electrode capacitance. Tip length is significant because this determines the physical strength of the electrode and how easily it will penetrate tissue and cells. A short tip with steep taper is robust but does not penetrate tissue easily. The converse is true of long gently tapering tips.

Tip diameter is important because it determines whether the electrode is suitable for intracellular recording or for patch recording. Intracellular recordings are made with electrodes having very narrow tips (approximately 0.1 micron), which can be obtained using a single-pull electrode puller. Generally, patch clamping requires a larger tip diameter of approximately 1 micron outside diameter and 0.5 micron inside diameter obtained using a double pull electrode puller. There is a correlation between tip length and distal tip diameter. For example, using a specific puller with varying heater widths and geometries, long tips were of narrower gauge at the ends than short tips (Flaming and Brown, 1982).

Capacitance and resistance are properties of the electrode that determine its confounding effect on measurements taken from neurons. In order to get accurate data, one needs to measure these properties and compensate for them. These properties are functions of the physical form of the electrode, the properties of the glass used to make it, and the electrolyte used to fill it. Therefore, since the manufacturing process determines this physical form, the process should be understood so that it can be tailored to create electrodes fitting the experimentalist's needs.

Capacitance and electrode resistance as a function of the pulling parameters can be measured but not at the same time as precise measurement of tip diameter or shank geometry. The procedure for measuring tip size accurately involves using the scanning electron microscope (SEM), which is time consuming and expensive. There are means to do this non-destructively (Fry, 1975). Other methods have been explored including measuring the rate of flow of a solution down the shank of an electrode and using a mathematical model to find tip size (Robinson and Scott, 1973). Mittman et al. (1987) used the pressure needed to

force bubbles from a microelectrode immersed in methanol to estimate tip diameter. From knowledge of the tip diameter and length of the electrode's tapering shank, capacitance has been computed using the approximation that the shank is a cone (Snell, 1969).

However, the exact relationship between the variables in the actual manufacturing process (heater geometry, rate of pulling the glass tube, length of first pull (for a patch electrode), rate of the second pull, etc.) and electrode properties is usually determined empirically by a method of trial-and-error. Though some work has been done on the influence of heater geometry and width on electrode form (Flaming and Brown, 1982), in general, the process is not well determined. In this paper, our objective is to develop a basic mathematical model for the formation process of these glass microelectrodes and, through computer simulations, understand the complex interaction of variables in the manufacturing process with the properties of the resulting electrode. This has the advantages that many different types of pullers can be simulated, the effects of many parameters can be explored rapidly, and predictions to guide the formation of microelectrodes using existing pullers as well as future design of electrode pullers can be made. There are several types of pullers in common use today. The differences between them include heater size and shape, method of application of the force (gravity, electromagnetic) to extend the glass tube, single and double pulls, and auxiliary cooling methods (e.g., puffs of air).

The main focus of this paper is on the pulling of glass microelectrodes. We will not analyze the rupture of the glass tube at the end of the pulling process. Instead, we will impose a breaking stress criterion to terminate the stretching of the glass tube when the viscous stress inside the glass tube exceeds the critical value of the stress, i.e., the breaking stress. However, the theory developed here can be generalized and applied to a broader class of problems. From the fluid dynamics point of view, the breaking of the glass tube may be due to the collapse of the glass wall. Furthermore, it also is possible that the inner radius of the glass tube shrinks to zero, resulting in failure of this production method to produce a functional electrode. Three major factors that determine these outcomes are the surface tension, viscous stress [tension], and pressure, which are all affected by the temperature of the glass. Previous studies of the stability of free surfaces of isothermal fluid jets as well as the effects of pressure and temperature may be used to predict the behavior of the surfaces in the stretched section of the glass tube. This will be the subject of a future paper.

The paper is organized as follows. In Section 2, the assumptions for the model and derivation of the model equations are given. Details of the control-volume approach used in this derivation are specified in Appendix A. The effects of thermal radiation from the coil heater on the glass tube requires the determination of the geometric factors from the coil and from the background to the glass, see Appendix B. Also described are the breaking stress criterion, which is used to terminate the numerical computations, and the glass properties used in the model. The added complication of a moving boundary due to the stretching of the glass tube is avoided by introducing a quasi-Lagrangian coordinate system. The actual length of the tube evolves according to a system of ordinary differential equations.

The finite-difference method is described in Section 3 and is used to compute the solutions numerically in space and time. In Section 4, several different cases of parameter values are

given as examples for the numerical computations, and results for a double pull case are described. The paper closes with a discussion in Section 5 on the limitation of the present model and future work for improving the model.

2 A Model for Glass Microelectrode Formation

2.1 Derivation of the model

In the model equations developed here for glass microelectrode formation, we account for certain types of electrode pullers which are capable of single and multiple pulls. The microelectrode starts off as a glass tube that is held vertically, being clamped at the top and with a weight hanging from the bottom, cf. Figure 1a. The tube then is heated nonuniformly in the longitudinal direction by radiation from an axially symmetric heated wire coil which surrounds the tube near the middle at the initial time. Also, there is radiation loss to the background, and we assume there is no radiant energy passing through the glass. The tube heats up to the softening point and begins to stretch due to the weight, cf. Figure 1b. Examination of microelectrodes formed in this way shows that symmetrical radial contraction of the glass tube occurs as longitudinal stretching takes place. Although this is a two-dimensional formation process, we treat the problem in one space dimension along the tube length by averaging over the cross-sectional area. This is justified because of the small diameter of the tube compared with the length of the tube.

In developing a mathematical model to describe the heating of a glass tube to form a microelectrode, we initially will be working with an Eulerian coordinate system with x and t as the spatial and temporal coordinates, respectively. The mass of the tube is small compared to the hanging weight w and will be ignored in the following derivation. At $t = 0$, we assume a uniform glass tube of length ℓ_0 with a circular annular cross-section having constant outer radius R_0 and constant inner radius r_0. The resulting area of the annular cross section is denoted by $s_0 = \pi(R_0^2 - r_0^2)$, and the coordinate along the glass tube is given by $0 \le x \le \ell_0$.

We assume that the stretching glass tube maintains a circular annular cross section with outer radius $R(x,t)$ and inner radius $r(x,t)$ at a given location x and time t (thus, $R_0 = R(x,0)$ and $r_0 = r(x,0)$). The cross-sectional area of the glass tube is given by $s(x,t) = \pi(R^2 - r^2)$ (thus, $s_0 = s(x,0)$). The length of the tube at time t is denoted by $\ell(t)$ (thus, $\ell_0 = \ell(0)$), and we refer to the location $x = \ell(t)$ as the "free end." The velocity of the glass at x at time t is given by $u(x,t)$. Thus the extensional strain rate is given by $\partial u/\partial x$, which corresponds to the spatial variation of the glass velocity.

From experiments, the dependence of density changes on temperature is negligible. Therefore, to simplify the model equations, we assume that the glass is an incompressible fluid with constant density and that the stretching is axial with concomitant shrinking of the cross-sectional area, $s(x,t)$. Using a control-volume approach (cf. Appendix A), we

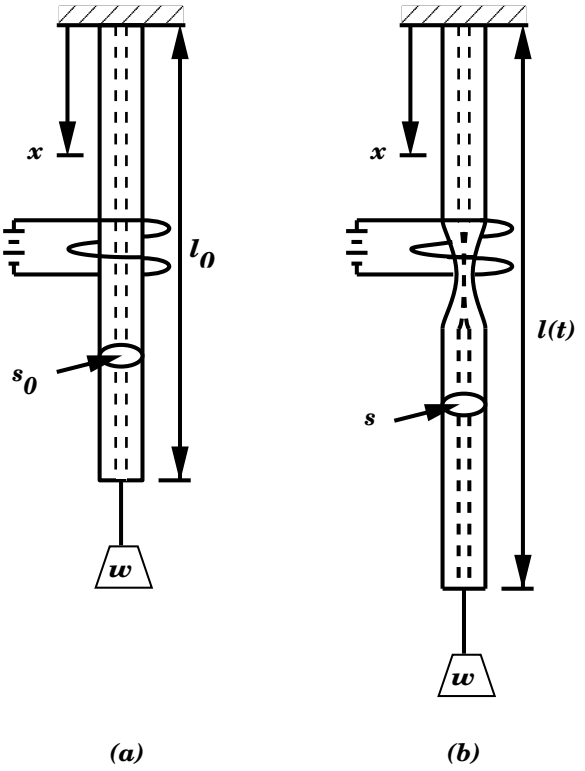

Figure 1: Schematics of the glass tube before (a) and during (b) the stretching.

have the continuity equation

$$\frac{\partial \gamma}{\partial t} + u\frac{\partial \gamma}{\partial x} + \gamma\frac{\partial u}{\partial x} = 0 \tag{2.1}$$

where $\gamma(x,t) = s(x,t)/s_0$.

The axial stress at each point in the glass tube is given by

$$\text{axial stress} = \frac{F}{s(x,t)} \tag{2.2}$$

where F is the axial force and is uniform over the length of the tube because we have neglected its mass[1]. To determine F, we use Newton's second law to describe the motion of the applied weight w

$$w - F = \frac{wa}{g} \tag{2.3}$$

where the acceleration $a = d^2\ell/dt^2$ is measured at the end of the glass tube, and g is the gravitational acceleration. Thus the glass satisfies the constitutive relation

$$\frac{w}{s(x,t)}\left(1 - \frac{a}{g}\right) = 3\mu\frac{\partial u}{\partial x} \tag{2.4}$$

[1]We refer the reader to Appendix A for more details.

where μ is the shear viscosity and 3μ is the coefficient of viscosity for axial tension. We have assumed that viscous stress is dominant over the inertia of the glass and the surface tension of the glass-air interface. Therefore, the Reynolds number, $Re = \rho\mathcal{U}\mathcal{L}/\bar{\mu}$, is small[2] where ρ is the glass density, and $\mathcal{U}$, $\mathcal{L}$, and $\bar{\mu}$ are the characteristic velocity, length, and viscosity, respectively. Note that $\mu = \mu(\theta(x,t))$ where $\theta(x,t)$ is the temperature of the glass at (x,t). The issue of surface tension is addressed briefly in Section 5.] Combining (2.1) and (2.4) yields

$$\frac{\partial \gamma}{\partial t} + u\frac{\partial \gamma}{\partial x} = -\frac{\mathcal{P}}{\mu}\left(1 - \frac{a}{g}\right) \tag{2.5}$$

where $\mathcal{P} \equiv w/3s_0 = \text{constant}$.

The temperature distribution $\theta(x,t),\ 0 < x < \ell(t),\ t > 0$, is subject to the initial condition $\theta(x,0) = \theta_0(x),\ 0 \le x \le \ell(0)$. We apply a standard control-volume method for deriving the energy equation (see Appendix A), resulting in

$$\rho\left(\frac{\partial c_p\theta}{\partial t} + u\frac{\partial c_p\theta}{\partial x}\right) = \frac{1}{s}\frac{\partial}{\partial x}\left(s\kappa(\theta)\frac{\partial \theta}{\partial x}\right) + E_R \tag{2.6}$$

where c_p and κ are the specific heat and thermal conductivity of the glass, respectively, and E_R represents the transport of thermal energy to the glass tube by radiation. This radiation term is given by

$$\begin{aligned} E_R &= 2k\sqrt{\frac{\pi}{s(1-\beta^2)}}\left[F_{hg}\frac{\varepsilon_h\alpha}{1-(1-\alpha)(1-\varepsilon_h)}\left(\theta_h^4 - \theta^4\right)\right. \\ &\quad \left. + F_{bg}\frac{\varepsilon_b\alpha}{1-(1-\alpha)(1-\varepsilon_b)}\left(\theta_b^4 - \theta^4\right)\right] \end{aligned} \tag{2.7}$$

where k is the Boltzmann constant, α is the absorptivity of the glass to radiative thermal energy, ε_h and ε_b are the emissivities of the heater and background, respectively, and $\theta_h(x,t)$ and $\theta_b(x,t)$ are the temperatures of the heater and the background, respectively. The quantities F_{hg}, F_{bg}, and F_{bh} are geometric factors between the heater and the glass tube, the background and the glass tube, and the background and the heater, respectively. We note that $F_{gh} = F_{hg}$, and similarly for the other two geometric factors. The derivation of the geometric factors is given in Appendix B. Finally, $\beta = r/R$ is the ratio of the inner and outer radii; thus $s = \pi R^2(1-\beta^2)$. In general, β is a function of x and t and can be determined by treating the interfaces between the glass tube and the air as free-boundaries. When the viscosity of the glass is small, i.e., the Reynolds number is large, it can be shown that β is approximately a constant, which is not the case for moderate and large values of the viscosity. A further discussion will be given in Section 4.

The initial conditions are given by $\theta(x,0) = \theta_0$, $\gamma(x,0) = 1$, and $u(x,0) = 0$. At the boundaries, $x = 0$ and $x = \ell(t)$, θ is fixed at θ_a, which is the ambient temperature. Since the boundary at $x = 0$ is fixed, the velocity $u(0,t) = 0$. At the moving boundary, $x = \ell(t)$,

[2]This assumption will be justified in the next section.

the velocity is given by $u(\ell(t),t) = d\ell(t)/dt$. In summary, the governing equations of our problem are the coupled equations, (2.5) and (2.6), with the specified initial and boundary conditions.

Finally, the criterion for determining when the glass tube breaks is the breaking stress for the glass. The maximal stress in the tube can be computed, and when it reaches the assumed breaking stress, the tube is considered broken. This procedure requires an accurate determination of the stress distribution in the tube both spatially and temporally because it varies rapidly as the tube thins down to small diameters. In the present study, we will find that in some cases, the breaking stress is not achieved after the maximum allowed extension of the glass tube is reached, and this results in an extremely fine tip with a long shank, which is not usable in experiments. When the breaking stress is achieved, the glass tube will break into two pieces, and the resulting shapes of the two electrodes produced then are determined.

3 Numerical Procedures

Since the governing equations are nonlinear, we seek the solution through numerical means. The main purpose of the numerical tests in this paper is to investigate the effects on the shape of the glass microelectrode tips obtained by changing the heater temperature θ_h. This parameter has been chosen since it is easy to adjust in the laboratory. We will simulate a typical two-pull electrode formation process used in the laboratory when the glass microelectrode is produced, which will be described briefly in the following.

3.1 Coordinate transformation

The moving boundary introduces an extra complication into the model even though the solution behavior is quite regular. To avoid this added complication in the numerical computations, we choose a quasi-Lagrangian coordinate system in which the moving boundary is fixed. However, this coordinate system does not follow the material motion as in true Lagrangian coordinates. This coordinate system can be obtained by a simple transformation from the Eulerian coordinates, which we now describe.

We derive the governing equations under the new coordinates (ξ,τ) defined by

$$\xi = \xi(x,t), \text{ or } x = X(\xi,\tau), \tag{3.1}$$

$$\tau = t, \tag{3.2}$$

where $\xi(0,t) = 0$ and $\xi(\ell(t),t) = 1$, and with new dependent variables

$$u(x,t) = U(\xi,\tau),\ \theta(x,t) = \Theta(\xi,\tau),\ \ell(t) = L(\tau), \tag{3.3}$$

$$a(t) = A(\tau),\ \gamma(x,t) = \Gamma(\xi,\tau),\ \mu(x,t) = \nu(\xi,\tau). \tag{3.4}$$

The relationships between the derivatives in the new (ξ,τ) and the old (x,t) coordinates are

$$\frac{\partial}{\partial x} = G\frac{\partial}{\partial \xi}, \tag{3.5}$$

$$\begin{aligned}\frac{\partial}{\partial t} &= \frac{\partial}{\partial \tau} - V\frac{\partial}{\partial x} \\ &= \frac{\partial}{\partial \tau} - VG\frac{\partial}{\partial \xi},\end{aligned} \tag{3.6}$$

where $V = \partial X/\partial \tau$ is the "grid velocity," and $G = \partial \xi/\partial x$ is the "reciprocal grid stretching ratio," which is to be specified.

From (2.4), we have

$$\frac{\partial u}{\partial x} = \frac{\mathcal{P}}{\gamma\mu}\left(1 - \frac{a}{g}\right), \tag{3.7}$$

and in the new coordinates, this becomes

$$\frac{\partial U}{\partial \xi} = \frac{\mathcal{P}}{G\Gamma\nu}\left(1 - \frac{A}{g}\right) \tag{3.8}$$

where $\nu = \gamma\mu$. The constitutive equation for γ, (2.5), under the transformation can be written as

$$\frac{\partial \Gamma}{\partial \tau} + (U - V)G\frac{\partial \Gamma}{\partial \xi} = -\frac{\mathcal{P}}{\nu}\left(1 - \frac{A}{g}\right). \tag{3.9}$$

The energy equation, (2.6), now is written in the new coordinates as

$$\rho\left(\frac{\partial c_p\Theta}{\partial \tau} + G(U - V)\frac{\partial c_p\Theta}{\partial \xi}\right) = G\Gamma\frac{\partial}{\partial \xi}\left(\frac{\kappa(\Theta)G}{\Gamma}\frac{\partial \Theta}{\partial \xi}\right) + E_R. \tag{3.10}$$

In order to solve (3.8) - (3.9), we need to compute conditions at the free end, $L(\tau)$. Integrating (3.8) from $\xi = 0$ to $\xi = 1$, and using $W(\tau) = U(1,\tau) = dL/d\tau$ and $dW/d\tau = A(\tau) = d^2L/d\tau^2$, we obtain

$$\frac{dL}{d\tau} = \left(1 - \frac{1}{g}\frac{d^2L}{d\tau^2}\right)\int_0^1 \frac{\mathcal{P}}{G\Gamma\nu}d\xi. \tag{3.11}$$

The information for the moving boundary (the length $L(\tau)$ and velocity $W(\tau)$) is obtained by solving a system of ordinary differential equations derived from (3.11)

$$\frac{dW}{d\tau} = g - \frac{1}{\mathcal{I}}W, \tag{3.12}$$

$$\frac{dL}{d\tau} = W, \tag{3.13}$$

where $\mathcal{I} = \int_0^1 \mathcal{P}/(\nu g G\Gamma)d\xi$.

3.2 Adaptive moving grid generation

A special feature of the problem being studied here is that the solutions (temperature, radius of the tube, etc.) vary rapidly in the region near the heater and much slower in regions away from the heater. A uniform grid results in unnecessarily dense grid points in some regions and not sufficiently dense in other regions. Therefore, an adaptive grid is desirable in the computation.

The approaches used in adaptive grid generation can be put into two general categories. When the grid generation and the physical equations are dealt with separately, the approach is called *static regridding*. This approach is usually robust and relatively simple to use. If the grid is generated simultaneously with the solution of the physical equations, then the approach belongs to the *moving mesh* methods.

We use a simple moving mesh method by solving a partial differential equation for the coordinate transformation

$$\xi = \xi(x,t), \tag{3.14}$$
$$\tau = t. \tag{3.15}$$

between the domian $\xi \in [0,1]$ and $x \in [0, L(\tau)]$. The differential equation, based on the Equi-distribution Principle, can be written as

$$\frac{\partial X}{\partial \tau} = \frac{1}{\tau_r}\frac{\partial}{\partial \xi}\left(M\frac{\partial X}{d\xi}\right), \quad 0 < \xi < 1. \tag{3.16}$$

Here τ_r is a (small) relaxation parameter and $M = \sqrt{(1+p\Gamma^{-2})/(1+\Gamma^{-2})}$ is the monitor function, which is chosen such that the grid is dense where Γ is small. The smoothing parameter p determines the ratio of finest and coarsest grid sizes, therefore prevents the distribution of too many points in the region when Γ is small. When solved numerically on a uniform grid $0 = \xi_0 < \xi_1 < \cdots < \xi_N = 1$, subject to the boundary conditions $X(0,\tau) = 0$ and $X_\tau(1,\tau) = U(1,\tau) = W(\tau)$ (or $X(1,\tau) = L(\tau)$), (3.16) generate a non-uniform grid $0 = x_0 < x_1 < \cdots < x_N = L(t)$.

We note that X must be a monotone function of ξ at any given time τ in order to be a coordinate transformation. This is guaranteed since equation (3.16) is a heat equation. Other equations and monitor functions can be used as well. For a detailed discussion, see [6] and references therein.

3.3 Finite-difference scheme

We solve the system (3.9) - (3.10) by a finite-difference method. We discretize (3.9) using a backward Euler scheme in time and an upwind difference in space, namely,

$$\Gamma_{i,n+1} - \Gamma_{i,n} = -\delta\tau\frac{\mathcal{P}}{\nu_{i,n+1}}\left(1 - \frac{A_{n+1}}{g}\right)$$

$$+\begin{cases} G_{i+1/2,n+1}(U_{i,n+1}-V_{i,n+1})(\Gamma_{i+1,n+1}-\Gamma_{i,n+1})\frac{\delta\tau}{\delta\xi} \\ \qquad \text{if} \quad U_{i,n+1}-V_{i,n+1}\le 0; \\ G_{i-1/2,n+1}(U_{i,n+1}-V_{i,n+1})(\Gamma_{i,n+1}-\Gamma_{i-1,n+1})\frac{\delta\tau}{\delta\xi} \\ \qquad \text{if} \quad U_{i,n+1}-V_{i,n+1}>0 \end{cases} \tag{3.17}$$

where $\delta\xi$ and $\delta\tau$ are the mesh and time step sizes, respectively, and i and n are the indices for the space coordinate and time level, respectively. For any grid function $f_{i,n}$, we define $f_{i+1/2,n}=(f_{i+1,n}+f_{i,n})/2$, $f_{i-1/2,n}=(f_{i-1,n}+f_{i,n})/2$. The reciprocal grid stretching ratio $G_{i,n}$ is computed using the standard central difference formula.

We now discretize (3.10) using a backward Euler scheme in time and central-differences in space, thus

$$\begin{aligned} \rho c_p\Theta_{i,n+1} &= \rho c_p\Theta_{i,n}-\frac{\rho c_p G_{i,n+1}\delta\tau}{2L_{n+1}\delta\xi}\left(U_{i,n+1}-V_{i,n+1}\right)\left(\Theta_{i+1,n+1}-\Theta_{i-1,n+1}\right) \\ &\quad +\frac{G_{i,n+1}\delta\tau}{\Gamma_{i,n+1}(L_{n+1})^2\delta\xi^2}\Big[\kappa_{i+1/2,n+1}\Gamma_{i+1/2,n+1}\left(\Theta_{i+1,n+1}-\Theta_{i,n+1}\right) \\ &\qquad -\kappa_{i-1/2,n+1}\Gamma_{i-1/2,n+1}\left(\Theta_{i,n+1}-\Theta_{i-1,n+1}\right)\Big] \\ &\quad +2k\delta\tau\sqrt{\frac{\pi}{S_0\Gamma_{i,n+1}(1-\beta^2)}}\left[F_{hg}\frac{\varepsilon_h\alpha}{1-(1-\alpha)(1-\varepsilon_h)}\left(\Theta_h^4-\Theta_{i,n+1}^4\right)\right. \\ &\qquad \left. +F_{bg}\frac{\varepsilon_b\alpha}{1-(1-\alpha)(1-\varepsilon_b)}\left(\Theta_b^4-\Theta_{i,n+1}^4\right)\right]. \end{aligned} \tag{3.18}$$

The equations describing the tip motion, (3.12) and (3.13), are solved in a different fashion. First of all, (3.12) is integrated from time level n (τ) to $n+1$ ($\tau+\delta\tau$) assuming that $\mathcal{I}$ is a constant in that time interval, which yields

$$W_{n+1}=g\mathcal{I}_{n+1}[1-\exp(-\delta\tau/\mathcal{I}_{n+1})]+W_n\exp(-\delta\tau/\mathcal{I}_{n+1}). \tag{3.19}$$

The acceleration then is obtained using (3.12) as

$$A_{n+1}=g-\frac{W_{n+1}}{\mathcal{I}_{n+1}}. \tag{3.20}$$

The tip length is obtained using a backward Euler method

$$L_{n+1}=L_n+W_{n+1}\delta\tau. \tag{3.21}$$

The trapezoidal rule is used to evaluate the integral

$$\mathcal{I}_{n+1}=\delta\xi\sum_{i=1}^{N}\frac{\mathcal{P}}{2g}\left(\frac{1}{G_{i,n+1}\Gamma_{i,n+1}\nu_{i,n+1}}+\frac{1}{G_{i-1,n+1}\Gamma_{i-1,n+1}\nu_{i-1,n+1}}\right). \tag{3.22}$$

Finally, the velocity at each interior point is computed by discretizing (3.8) using the trapezoidal rule

$$\begin{aligned} U_{i,n+1} &= U_{i-1,n+1} \\ &\quad +\delta\xi\frac{\mathcal{P}}{2}\left(1-\frac{A_{n+1}}{g}\right)\left(\frac{1}{G_{i,n+1}\Gamma_{i,n+1}\nu_{i,n+1}}+\frac{1}{G_{i-1,n+1}\Gamma_{i-1,n+1}\nu_{i-1,n+1}}\right). \end{aligned} \tag{3.23}$$

The mesh adaptation also is done numerically. The finite-difference approximation of equation (3.16) is

$$\begin{aligned} X_{i,n+1} &= X_{i,n}+\frac{\delta\tau}{\tau_r(\delta\xi)^2}\Big[M_{i+1/2,n+1}(X_{i+1,n+1}-X_{i,n+1}) \\ &\quad -M_{i-1/2,n+1}(X_{i,n+1}-X_{i-1,n+1})\Big]. \end{aligned} \tag{3.24}$$

The boundary conditions for (3.24) are

$$X_{0,n+1}=0, \quad X_{N,n+1}=L_{n+1}.$$

3.4 Solution algorithm

For the initial conditions, we assume that the glass tube has uniform properties and constant temperature distribution with no motion. Since the equation for temperature is second-order in space, we need two boundary conditions, namely, the Dirichlet conditions that the temperature is held fixed at both ends. The equation for Γ is first-order in space, which means that normally one condition needs to be specified. However, $U-V=0$ at both ends, so the characteristic curve at each boundary point, $\xi=0$ and 1, is tangent to the boundary. Therefore, no explicit boundary conditions are needed for Γ. Furthermore, $U_{0,n+1}=0$, which is sufficient to solve for $U_{i,n+1}$.

We assume that the values of the variables at time level n are known, and we use an iterative procedure for solving the discrete equations for these variables at time level $n+1$:

1. the temperature Θ is computed using (3.18);
2. the value of $\mathcal{I}$ is calculated using (3.22);
3. then, W, A, and L are obtained from (3.19), (3.20), and (3.21), respectively;
4. the values of Γ are computed from (3.17);
5. the velocity U is determined from (3.23); and
6. after the physical equations are solved, we update the mesh by solving the mesh equation (3.24), then move to the next time level.

Using these values of the variables, we update the coefficients, e.g., ν, etc., in the discrete equations, and repeat steps 1-6 until convergence is achieved. These computations are repeated until either the maximum extension length is reached or the breaking stress in the glass tube is exceeded.

We note that our numerical method is implicit and an iterative procedure is required due to the nonlinear nature of the physical and grid generation equations. In principle, a simpler explicit method also can be used to solve the set of equations listed above. However, such methods normally impose a severe constraint on the size of the time step even for linear problems. On the other hand, we can choose a relatively large step size by using the implicit method. The iterative procedure at each time step usually converges with only a few iterations.

Most of the results presented in the following section are obtained using 512 grid points in the spatial discretization. We have experimented with more grid points but the results are essentially the same. The size of the time step, which is allowed to vary in our computations, is chosen according to the velocity of the glass so that the free-end of the glass moves less than 10^{-3} of the initial tube length ℓ_0.

4 Results

To illustrate the theory developed in this paper, we have carried out several representative computations of glass microelectrode formation. For patch-clamp experiments, appropriate strength in the shank of the electrode requires two separate pulls with different heater temperatures. Therefore, the first pull with heater temperature, θ_h^1, is stopped when the glass tube is extended to a certain length and forms a 'neck'. The heater is switched off, and switched on again, usually at a lower temperature θ_h^2, after it has been moved to a location approximately at the smallest part of the neck and the glass tube has cooled down. The glass tube usually breaks during the second pull with the desired tip shape if the temperature of the heater is set properly. A maximum extension length, which is determined by the dimension of the puller, is set for the second pull. The adjustable parameters are the temperature, the location of the heater, and the force load on the end of the tube. The computations were carried out for two different values of θ_h^1 for the first pull, combined with various heater temperatures θ_h^2 for the second pull.

Since the ratio of the inner and outer radii of the tube, $\beta = r/R$, is treated as an unknown function in our model, we considered two cases. The first set of computations were carried out assuming that β is a constant, which is valid when the viscosity is relatively small. For the second set of computations, we assumed that β is a linear function of the non-dimensional area Γ

$$\beta = \frac{1}{2} + \beta_0(\Gamma - 1) \tag{4.1}$$

where β_0 is a constant. We note that neither of these assumptions on β may be realistic. However, the computations based on these assumptions will provide useful information on

Table 1: *List of the physical parameters used in the computations.*

ρ gm/cm^3	c_p Erg/Kgm	κ cm^2/sec	k Erg/cm^2secK^4	ε_h cm^2/gm	ε_h cm^2/gm	α cm^2/gm
2.23	7.538×10^6	1.130×10^5	5.67×10^{-5}	1	1	0.4

the limitations and effects of β on the shape of the electrode when other parameters remain unchanged.

We carried out a number of numerical computations for the double-pull paradigm. The objective in the double-pull cases was to obtain tip diameters of approximately 1 μm. The important parameter was the heater temperature which can be controlled in experiments and was varied in the computations. We first describe the properties of the glass tubes used in the numerical computations and then present the results of these computations for the glass shapes, temperature distributions, stress distributions, and their time evolutions.

4.1 Glass properties and geometrical parameters

We first describe the relevant physical and geometrical parameters. The nonlinear dependence on temperature of the coefficients in the governing equations is determined by experimental measurements. In order to follow the physical process as closely as possible, we estimate the parameter values from these data.

The most important parameter is the viscosity of the glass, μ. According to the measurements, the relationship between $\ln \mu$ and the temperature is piecewise linear. Therefore, we use power laws for the temperature dependence over certain intervals. A typical formula for the viscosity of the glass ($gm/cm\ sec$) is given by

$$\mu(\theta) = \begin{cases} 10^{9-c_1(\theta-293)} & \theta \le 900, \\ 10^{3.612-c_2(\theta-900)} & 900 \le \theta \le 1100, \\ 10^{3.38-c_3(\theta-1100)} & 1100 \le \theta \le 1500. \end{cases} \tag{4.2}$$

Here $c_1 = 8.876 \times 10^{-3}, c_2 = 1.16 \times 10^{-3}$, and $c_3 = 7.355 \times 10^{-3}$, based on measurements for soda-lime [8]. The other physical parameters used in our computations also come from the experimental setup, which are summarized in Table 1. The initial temperature of the glass tube is set to be the background temperature, or the room temperature (assumed to be 20° C), i.e., $\theta_0 = \theta_b = 293°$ K.

The geometrical parameters for the glass tube and heater are given in Table 2. The other two relevant parameters are ℓ_{p1} and ℓ_{p2}, which are the maximum lengths set for the first and second pulls, respectively. Due to the physical constraint of the puller, $\ell_{p1}+\ell_{p2}$ is usually fixed while various combinations are allowed. In this study, however, we have chosen $\ell_{p1} = 0.58\ cm$ and $\ell_{p2} = 4\ cm$. The initial area is $s_0 = \pi(R_0^2 - r_0^2) = \pi R_0^2(1 - \beta_0^2) = 1.767 \times 10^{-2}$.

During the pulling processes, the glass tube usually breaks in the location where the stress exceeds the "breaking stress". The breaking stress is a material-dependent parameter

Table 2: *List of the geometrical parameters used in the computations.*

Glass Properties			Heater Properties		
ℓ_0	R_0	r_0	x_h	ℓ_h	R_h
cm	cm	cm	cm	cm	cm
7.56	8.66×10^{-2}	4.33×10^{-2}	3.63	0.3	0.15

Table 3: *'NB' stands for the cases when the breaking stress criterion is not met; superscript 'e' denotes the values at the end of the second pull, and superscript 'b' denotes the values when the maximum stress $\mathcal{S}_{max}$ first exceeds the breaking stress $\mathcal{S}_b$; R_{min} and r_{min} are the outer and inner radii of the glass at the neck.*

θ_h^1 (K^o)	1100			1500		
θ_h^2 (K^o)	900	1100	1500	900	1100	1500
$\mathcal{S}_b^e$ $(\times 10^9\ dyn/cm^3)$	2.41	2.26	2.10	2.45	2.33	2.17
$\mathcal{S}_{max}^e$ $(\times 10^9\ dyn/cm^3)$	4.89	1.88	.350	7.49	3.48	.726
R_{min}^e (μm)	12.4	6.67	5.35	5.98	3.75	2.71
r_{min}^e (μm)	6.19	3.33	2.68	2.99	1.88	1.35
$\mathcal{S}_b$ $(\times 10^9\ dyn/cm^3)$	2.40	NB	NB	2.44	2.30	NB
$\mathcal{S}_{max}^b$ $(\times 10^9\ dyn/cm^3)$	2.41	NB	NB	2.49	2.31	NB
R_{min}^b (μm)	51.2	NB	NB	55.3	43.0	NB
r_{min}^b (μm)	25.6	NB	NB	27.6	21.5	NB

that also depends on the temperature. For example, for the glass used in this study, the breaking stress (in dyn/cm^3) is given by the empirical formula (Scholze, 1990)

$$\mathcal{S}_b = \frac{5.12 \times 10^{10}}{\sqrt{\theta}}, \tag{4.3}$$

which indicates that it becomes easier to break this type of glass as the temperature increases. For our first set of computations with a constant β, we choose not to impose the breaking stress. Instead, we use the maximum length $\ell_{p1} + \ell_{p2}$ as a stopping criterion. The breaking stress using (4.3) is computed as reference values. The breaking stress criterion is imposed for the second set of computations when β is a function of Γ (4.1).

4.2 Numerical results for constant β

In Table 3, we summarize the computational results based on the constant area ratio $\beta = 1/2$. The table lists the minimum radii (the values at the "neck" of the tube) and the maximum stress at the ends of the first and the second pulls, and when the stress in the glass tube

Table 4: *'NB' stands for the cases when the breaking stress criterion is not met; superscript 'b' denotes the values when the maximum stress $\mathcal{S}^b_{max}$ first exceeds the breaking stress $\mathcal{S}_b$; R^b_{min} and r^b_{min} are the outer and inner radii at the neck; t is the time from the start of the second pull; and x_{min} is the location of the neck from the clamped end of the glass.*

θ^1_h (K^o)	1100				1500			
θ^2_h (K^o)	900	1042	1044	1046	1100	1190	1192	1194
$\mathcal{S}_b$ $(\times 10^9\ dyn/cm^3)$	2.40	2.28	2.28	NB	2.30	2.25	2.25	NB
$\mathcal{S}^b_{max}$ $(\times 10^9\ dyn/cm^3)$	2.41	2.28	2.28	NB	2.31	2.25	2.25	NB
R^b_{min} (μm)	51.2	19.6	17.7	NB	43.0	18.1	15.6	NB
r^b_{min} (μm)	25.6	9.81	8.87	NB	21.5	9.01	7.78	NB
t^b (sec)	12.8	9.97	9.95	NB	3.05	2.80	2.80	NB
x^b_{min} (cm)	4.59	4.92	4.99	NB	4.31	4.58	4.65	NB

exceeds the breaking stress computed using formula (4.3). The heater temperatures for the two pulls are chosen to be a combination of 900 K, 1100 K, and 1500 K, since these are the critical values for the glass viscosity shown in (4.2).

The first observation one can make is that critical heater temperatures exist, i.e., temperatures beyond which the stress in the glass tube never reaches the breaking stress. It also can be seen that radii at the end of the second pull do not vary significantly. However, the value of maximum stress that exceeds the breaking stress, for some of the cases listed, is affected by the heater temperature. This suggests that if the breaking stress criterion is imposed, then the glass tube may break and the minimum radii (at the neck) of the tube may vary. This is confirmed by the values of the radii when the stress first exceeds the breaking stress. In all the cases, the radii at the end of the second pull are comparable to the values for the glass electrodes pulled in the laboratory. However, the radii when the stress exceeds the breaking stress on the first pull are much larger than those at the end of the second pull.

To further investigate the dependence of the minimum radii on the heater temperature, we have done simulations with careful variations of the temperature. The results are given in Table 4. With small variations of the heater temperature, we numerically identified the critical temperatures for the second pull. For $\theta^1_h = 1100\ K^o$, this critical temperature is about $\theta^2_h = 1044\ K^o$, whereas for $\theta^1_h = 1500\ K^o$, this critical temperature is about $\theta^2_h = 1192\ K^o$. In general, the neck radii are sensitive to the heater temperature. However, when the glass breaks (breaking stress is reached) at the critical heater temperatures during the second pull, the radii of the neck appear to be less sensitive to the heater temperature of the first pull.

The time history of the stress and breaking stress offers a clearer picture of what happens near the critical temperature, as plotted in Figure 2 for $\theta^1_h = 1500\ K^o$. It can be seen that during the second pull, the breaking stress decreases initially, reaches a minimum value, and then starts to increase again. This apparently corresponds to the fact that the temperature at the neck rises first, reaches a maximum, and then decays when the neck moves away from

the center of the heater. In the cases shown in Figures 2a, b, c, at a relatively low heater temperature ($\theta_h^2 = 1100\ K^o$), the stress at the neck of the glass tube increases monotonically with time and passes the breaking stress during the second pull. At a higher heater temperature ($\theta_h^2 = 1500\ K^o$), the maximum stress increases initially, reaches a maximum value, and then decreases. It never reaches the breaking stress (Figure 2d). Note that the peak of the maximum stress, just before breaking, decreases with increasing temperature during the second pull. Deceasing the heater temperature raises the maximum value of the stress (Figure 2a). As a result, the stress reaches and passes the breaking stress sooner for lower heater temperature during the second pull. Therefore, the neck radii are greater at lower heater temperature during the second pull when the breaking stress is met since there is insufficient time for the tube to stretch and reduce the neck radii. This is demonstrated in Figure 3 where the outer radius of the neck is plotted against time.

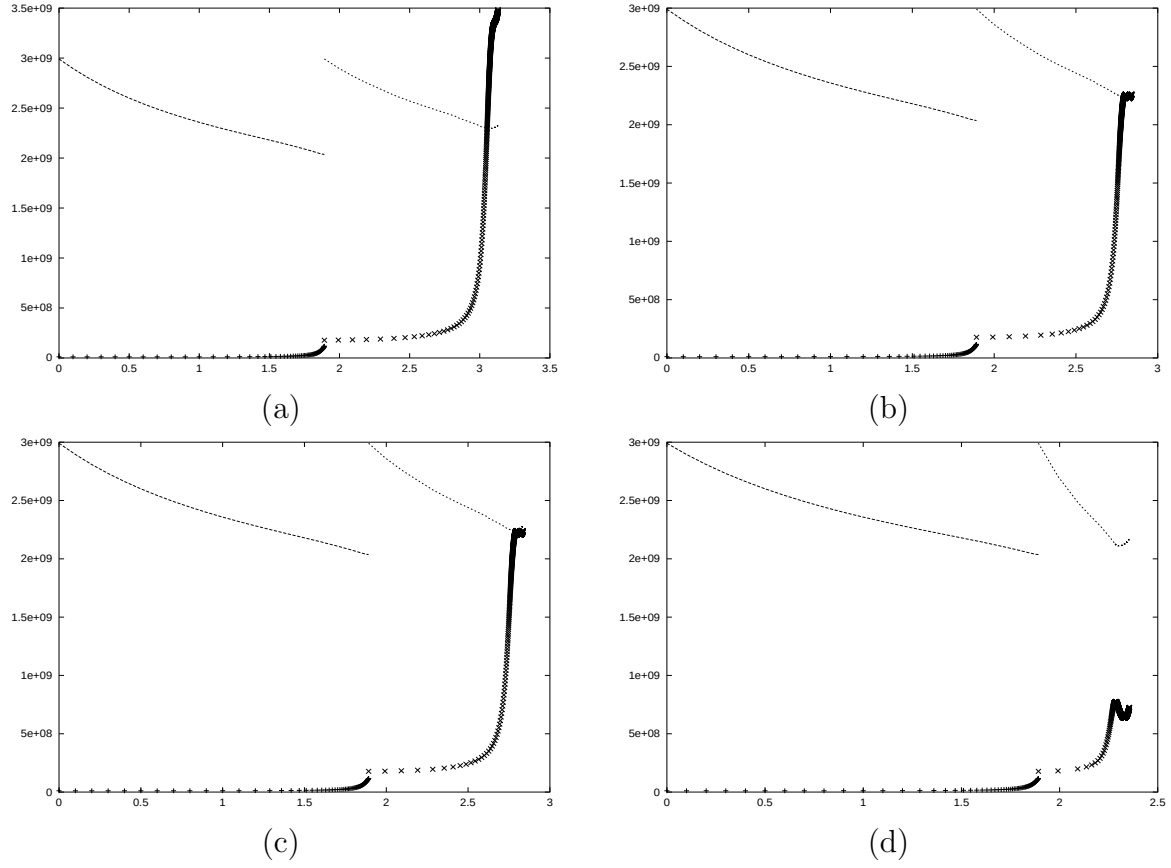

Figure 2: *Stress and breaking stress (in dyn/cm^3) versus time with θ_h^1=1500 K^o and (a) θ_h^2=1100 K^o; (b) θ_h^2=1192; (c) θ_h^2=1194 K^o; (d) θ_h^2=1500 K^o. The dashed line denotes the breaking stress and the symbols ($\times$ and $+$) are the maximum stresses.*

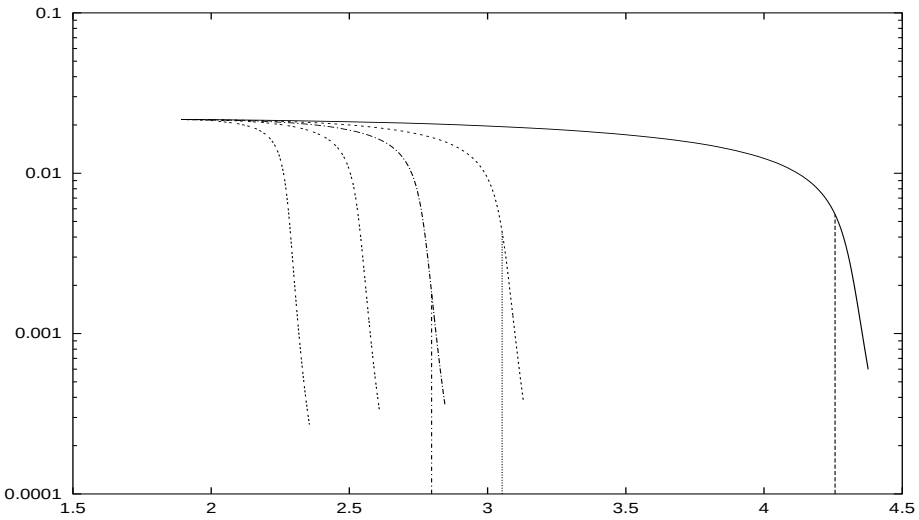

Figure 3: *Neck outer radius (in cm) versus time (in sec) with the same heater temperature* Θ_H^1*=1500* K^o *for the first pull and* θ_h^2*=900, 1100, 1190, 1300, and 1500* K^o *for the second pull, ordered from right to left. The times when the maximum stress exceeds the breaking stress and the corresponding values of the radii are marked. These times depend on the heater temperature during the second pull.*

4.3 Numerical results for variable β

In order to gain some insight on the effect of β, the ratio of the inner and outer radii of the glass tube, we present some computations with $\theta_h^1 = 1500\ K^o$ and $\theta_h^2 = 1190\ K^o$ with β given by (4.1) where β_0 varies from 0.3 to -0.2. The breaking stress criterion is imposed, and the glass breaks for every value of β_0. In Table 5, we have listed the outer and inner radii and the dimensionless area at the tip (neck) as well as the minimum value of β when the glass tube breaks. Note that γ is initially 1, so β is initially 0.5 for the first pull. However, the value of γ is negligible in determining β_{min} when the glass tube breaks, cf. (4.1) and Table 5. Clearly, the value of β_0 (therefore the value of β) has a visible effect on the values of the tip radii and area. It can be seen that the tip area decreases monotonically as β_0 decreases. However, the actual values of the tip outer and inner radii vary in a more complicated fashion. We note that the effect of β_0 (and β) is more effective in reducing R_{min} and r_{min} when $\beta_0 \leq 0$ ($\beta_{min} \geq 0.5$). There seems to exist a β_0 value between 0 and -0.2 (correspondingly $\beta_{\min}$ is between 0.5 and 0.7) for which both radii at the tip are reduced by about a factor of 3-4 (close to their respective local minima). This corresponds to the case where the inner radius contracts slower than the outer radius, resulting in a smaller tip area. On the other hand, if the inner radius contracts faster than the outer one ($\beta < 0.5$), the effects of different β_0 (β) on the inner radius is clearly demonstrated, while the effects on the tip area and its outer radius are limited as β_0 increases ($\beta_{\min}$ decreases).

Finally in Figure 4, we plot the corresponding shape of the glass tube for three of the cases computed when the breaking stress is reached. It can be seen that smaller values of

Table 5: Tip geometry as a function of β. The temperatures of the heater are 1500 K^o for the first pull and 1190 K^o for the second pull. Radii are given in μm. The minimum value of the reciprocal grid stretching ratio is given in the second column.

β_0	$G_{\min}$	$R_{\min}$	$r_{\min}$	$\beta_{\min}$
0.3	1.20×10^{-3}	26.5	5.32	0.20
0.2	1.10×10^{-3}	26.1	7.84	0.30
0.1	9.33×10^{-4}	25.0	10.0	0.40
0.0	4.34×10^{-4}	18.1	9.03	0.50
-0.1	1.51×10^{-5}	3.64	2.19	0.60
-0.2	1.31×10^{-5}	3.80	2.66	0.70

the tip radii, when $\beta_0 = -0.1$, are due mainly to the time available for the glass to stretch.

5 Concluding Remarks

In this study, we present a mathematical model for the formation of glass microelectrodes using a double pull paradigm. The model is one dimensional and is based on the assumption that the glass material is an incompressible viscous fluid. Numerical results indicate that the heater temperature plays a critical role in the formation process. In order to obtain glass electrodes with desirable tip shape and dimension, one needs a suitable combination of the heater temperature for the two pulls. Another important factor revealed by our model and the numerical simulations is the ratio of the inner and outer radii, β. Since our model does not take the free-boundary into account, this ratio remains a free parameter. The effect of β is investigated by using a simple linear relationship between β and the dimensionless area γ, which can be viewed as the first-order approximation when γ is close to its initial value. It is shown that changing the value of β has little effect on the results when the inner radius contracts faster than the outer one. On the other hand, both the inner and outer radii at the tip could be reduced by a factor of four or more if the inner radius contracts slower than the outer one. We also have investigated the effects of surface tension. It was found that under the physical conditions, surface tension is at least one magnitude smaller than the viscous stress. Therefore, excluding the effect of surface tension in the current model is justified.

Although our focus here has been on the specific manufacturing paradigm for glass microelectrodes in the laboratory, our mathematical model does allow us to investigate a variety of other possible changes in the parameters to obtain better shaped microelectrodes, e.g., the effects of changes in the weight, the ambient temperature, and different pulling strategies.

However, a more conclusive result only can be obtained from a more realistic model which takes the free-boundary into account. Work is currently underway to incorporate the effects

of surface tension and pressure changes due to temperature variations into the current model.

Acknowledgment We wish to thank Dr. Hilton Ramsey for several useful discussions in the early part of this research. Also, we thank Ken Burkett and Bruce Walding of Corning Glass for supplying us with the thermal and mechanical properties of Corning glass. This research was supported in part by research grants to HH and RMM from the Natural Sciences and Engineering Research Council (NSERC) of Canada.

References

[1] A.D. Fitt, K. Furusawa, T.M. Monro, and C.P. Please, *Modeling the fabrication of hollow fibers: Capillary drawing,* J. Lightwave Technol., 19 (2001), pp. 1924-1931.

[2] D.G. Flaming and K.T. Brown, *Micropipette puller design, form of the heating filiment and effects of filiment width on tip length and diameter,* J. Neurosci. Methods, 6 (1982), pp. 91-102.

[3] D.M. Fry, *A scanning electron microscope method for the examination of glass microelectrode tips either before or after use,* Experientia, 31 (1975), pp. 695-697.

[4] P. Gospodinov and A.L. Yarin, *Draw resonance of optical microcapillaries in nonisothermal drawing,* Int. J. Multiphase Flow, 23 (1997), pp. 967-976.

[5] J.R. Howell, *A Catalog of Radiation Configuration Factors,* McGraw-Hill, New York, 1982.

[6] W. Huang, Y. Ren, and R.D. Russell, *Moving mesh PDEs based on the equidistribution principle,* SIAM J. Numer. Anal., 31 (1994), pp. 709-730.

[7] S. Mittman, D.G. Flaming, D.R. Copenhagen, and J.H. Belgum, *Bubble pressure measurement of micropipette tip outer diameter,* J. Neurosci. Methods, 22 (1987), pp. 161-166.

[8] *Pyrex Glass Code 7740, Material Properties*, Brochure Pyrex B-87, 1987.

[9] G.R. Robinson, and B.I.H. Scott, *A new method of estimating micropipette tip diameter,* Experientia, 29 (1973), pp. 1039-1040.

[10] H. Scholze, *Glass, Nature, Structure, and Properties*, translated by M.J. Lakin, Springer-Verlag, New York, 1990, pp. 255-272.

[11] E.M. Snell, *Some electrical properties of fine tipped pipette microelectrodes,* in Glass Microelectrodes, edited by M. Lavallee, A.F. Shanne, and N.C. Hubert, Wiley, New York, 1969, pp. 111 ff.

[12] A.L. Yarin, P. Gospodinov, and V.I. Roussinov, *Stability loss and sensitivity in hollow fiber drawing,* Phys. Fluids, 6, pp. 1454-1463.

Appendix A Derivation of the Model

To derive both the continuity equation (2.1) and the energy equation (2.6) for the glass tube, we apply a control-volume approach. Figure 5 is a schematic diagram of a typical infinitesimal section of the glass tube with length Δx. The control volume consists of four surfaces: two annuli with areas $s(x,t)$ on the left side and $s(x+\Delta x,t)$ on the right side, and outer and inner surfaces with areas given approximately by $s_{\text{out}} = 2\pi R(x,t)\Delta x$ and $s_{\text{in}} = 2\pi r(x,t)\Delta x$ where R and r are the radii of the outer and inner circles on the left side, respectively. We assume that the effect of the local slopes with respect to x of the outer and inner radii are negligible.

The conservation of mass, i.e., the net change of the glass in the control volume due to the net flux of glass from the left and right sides, is given by the continuity equation

$$\frac{\partial(\rho s)}{\partial t} + \frac{\partial(\rho s u)}{\partial x} = 0 \tag{A.1}$$

where ρ is the glass density and u is the local velocity. With the incompressibility assumption, i.e., the material derivative of the density is $D\rho/Dt = \partial\rho/\partial t + u\partial\rho/\partial x = 0$, the continuity equation can be simplified to

$$\frac{\partial s}{\partial t} + \frac{\partial(su)}{\partial x} = 0. \tag{A.2}$$

Define $\gamma \equiv s/s_0$ where s_0 is the initial constant annular cross-sectional area of the tube. Then (A.2) becomes

$$\frac{\partial \gamma}{\partial t} + u\frac{\partial \gamma}{\partial x} + \gamma\frac{\partial u}{\partial x} = 0. \tag{A.3}$$

In order to write down the conservation law for the energy, we make the following observations:

1. On the left surface, the energy influx is due to convective flow of the glass and conduction of heat through the glass within a period Δt, which is given by

$$E^{\text{in}} = s\left(\rho c_p u\theta - \kappa\frac{\partial\theta}{\partial x}\right)\Delta t \tag{A.4}$$

where c_p, κ, and θ are the specific heat, thermal conductivity, and temperature of the glass, respectively. The first term on the right-hand side is the convection due to motion of the glass, and the second term is the heat conduction using Fourier's law.

2. On the right surface, the energy outflux can be written similarly as

$$E^{\text{out}} = -s\left(\rho c_p u\theta - \kappa\frac{\partial\theta}{\partial x}\right)\Delta t - \frac{\partial}{\partial x}\left[s\left(\rho c_p u\theta - \kappa\frac{\partial\theta}{\partial x}\right)\right]\Delta x\Delta t. \tag{A.5}$$

The minus signs reflect the fact that energy is being removed.
3. On the outer surface, the energy exchange mechanism is mainly radiation between the heater coil, glass pipette, and background. For a differential cross-section of the tube, the radiative heat transfer absorbed at the surface is given by

$$E^{\text{rad}} = s_{\text{out}} \left[F_{hg} \frac{\varepsilon_h \alpha}{\varepsilon_h + \alpha - \varepsilon_h \alpha} (\theta_h^4 - \theta^4) + F_{bg} \frac{\varepsilon_b \alpha}{\varepsilon_b + \alpha - \varepsilon_b \alpha} (\theta_b^4 - \theta^4) \right], \tag{A.6}$$

where we have assumed the standard fourth-power law of surface-to-surface radiative heat transfer. The factors F_{hg} and F_{bg} are geometrical factors related to the relevant surfaces. In this case, they are the heater surface, the glass outer surface, and the background. Therefore, the subscripts hg and bg refer to the relationship between the heater and glass surfaces and the background and glass surfaces, respectively. The detailed derivations of these factors are given in Appendix B. The parameters $\varepsilon_h, \varepsilon_b$, and α are the emissivities for the heater and the background, and the absorptivity of the glass, respectively. The first term is the amount of the net energy flux absorbed by the outer surface of the glass tube, due to the radiation from the heater, which is at the temperature $\theta_h \geq \theta$. The second term is the net energy radiated away from the glass tube towards the background, which is at the temperature $\theta_b \leq \theta$.
4. There is no net energy exchange through the inner surface of the glass.
5. The incremental change in the internal energy within the control-volume of the glass tube is determined by the change of temperature during the time period Δt and is given by

$$E^{\text{int}} = [\rho c_p s(x, t + \Delta t)\theta(x, t + \Delta t) - \rho c_p s(x, t)\theta(x, t)]\Delta x. \tag{A.7}$$

With these assumptions, we can write down the equation for the temperature using the conservation of energy, i.e., the net increase in the internal energy is equal to the net flux of energy into the control volume, thus (A.7) = (A.4) + (A.5) + (A.6). After rearranging the terms, we obtain

$$\begin{aligned} \frac{\partial \rho c_p s\theta}{\partial t} + \frac{\partial \rho c_p su\theta}{\partial x} &= \frac{1}{s}\frac{\partial}{\partial x}\left(s\kappa(\theta)\frac{\partial \theta}{\partial x} \right) \\ &\quad + 2\sqrt{\frac{\pi}{s(1-\beta^2)}} k \left[F_{hg} \frac{\varepsilon_h \alpha}{\varepsilon_h + \alpha - \varepsilon_h \alpha} (\theta_h^4 - \theta^4) \right. \\ &\quad \left. + F_{bg} \frac{\varepsilon_b \alpha}{\varepsilon_b + \alpha - \varepsilon_b \alpha} (\theta_b^4 - \theta^4) \right]. \end{aligned} \tag{A.8}$$

We have assumed that the ratio of the inner and outer radii, $\beta = r/R$, is a constant independent of t and x. Note that this equation is different from (2.6) used in our computations. Equation (A.8) is written in conservation form while (2.6) is in non-conservative form. In (A.8), we can rewrite the two terms on the left-hand side as

$$\begin{aligned} \frac{\partial \rho c_p s\theta}{\partial t} + \frac{\partial \rho c_p su\theta}{\partial x} &= \rho s \left(\frac{\partial c_p \theta}{\partial t} + u \frac{\partial c_p \theta}{\partial x} \right) + c_p \theta \left(\frac{\partial (\rho s)}{\partial t} + \frac{\partial \rho s u}{\partial x} \right) \\ &= \rho s \left(\frac{\partial c_p \theta}{\partial t} + u \frac{\partial c_p \theta}{\partial x} \right) \end{aligned}$$

where we have used the continuity equation (A.1). Therefore, the conservation form (A.8) and non-conservative form (2.6) of the energy equation are equivalent.

Appendix B Derivation of Geometric Factors

The derivation of the equation for the transfer of thermal energy from the coil heater to the glass tube through radiation requires a detailed knowledge of the differential radiation from a differential area element on the inside surface of the heater to a differential area element on the outer surface of the glass tube. It is assumed that there is no radiation passing through the tube itself. The glass tube surface is assumed to have an absorptivity equal to α. Also, we take into account the variations of the inner and outer radii of the tube. However, we assume that the effects due to the local slope of the outer radius with respect to x are negligible. Also, we approximate the coil by a cylindrical surface with emissivity ε_h.

To account for the relative surface orientations of the heater and tube surfaces, we compute the geometric (or radiation configuration) factor needed to evaluate the thermal energy transfer to the tube (Howell, 1982). The geometry of the heater and tube system and the notation are shown in Figure 6. We evaluate the total radiative heat transfer from the heater to a differential cross-section of the tube centered at x. The differential of the geometric factor for a differential area ds at x on the tube for a differential area ds_h on the heater is given by

$$dF_{hg} = \frac{\cos\phi \cos\phi_h ds ds_h}{\pi\sigma^2}$$

where ϕ and ϕ_h are the angles of the line (of length σ) connecting the differential area elements ds and ds_h with the outer normal of the glass tube and inner normal of the heater, respectively. The differential area element on the heater is

$$ds_h = R_h dy d\Phi$$

where R_h is the heater radius, y is the axial distance between the differential area elements, and Φ is the angle between the two radial segments show in Figure 6. Thus the geometric factor from the heater to the area element ds is given by

$$\begin{aligned} F_{hg} &= \frac{1}{\pi}\iint \frac{\cos\phi\cos\phi_h}{\sigma^2} ds_h \\ &= \frac{1}{\pi}\int_{-\Phi_0}^{\Phi_0}\int_0^{\ell_h} \frac{\cos\phi\cos\phi_h}{\sigma^2} R_h dy d\Phi \end{aligned} \tag{B.1}$$

where

$$\begin{aligned} \cos\phi &= -\frac{R^2+\sigma^2-(\ell_h^2+R_h^2)}{2R\sigma}, \\ \cos\phi_h &= \frac{R_h^2+\sigma^2-(\ell_h^2+R_h^2)}{2R_h\sigma}, \end{aligned}$$

$$\begin{aligned}\sigma^2 &= (y + x_h - x)^2 + R^2 + R_h^2 - 2RR_h \cos\Phi, \\ \Phi_0 &= \cos^{-1}\left(\frac{R}{R_h}\right). \end{aligned} \tag{B.2}$$

The double integral for the geometric factor (B.1) can be simplified to a single integral

$$\begin{aligned} F_{hg} &= -\frac{1}{\pi}\int_0^{\Phi_0} R_h(R_h - R\cos\Phi)(R - R_h\cos\Phi) \\ &\quad \cdot \left[\frac{y + x_h - x}{\mathcal{R}^2[(y + x_h - x)^2 + \mathcal{R}^2]} + \frac{\tan^{-1}\frac{y+x_h-x}{\mathcal{R}}}{\mathcal{R}^3}\right]_{y=0}^{y=\ell_h} d\Phi \end{aligned} \tag{B.3}$$

where

$$\mathcal{R}^2 = R^2 + R_h^2 - 2RR_h\cos\Phi.$$

The geometric factor between the glass tube and the background is equivalent to the geometric factor between the glass tube and an infinite cylindrical shell where the segment shielded by the heater is excluded. The formula for this geometric factor can be obtained more simply by replacing the cylinder with a spherical shell, again excluding the portion of the shell shielded by the heater. This formula is given by

$$F_{bg} = 1 - \frac{1}{2\pi}[2(\beta_2 - \beta_1) + \sin 2\beta_2 - \sin 2\beta_1] \tag{B.4}$$

where $\beta_1 = \arctan\frac{R_h}{x_h}$ and $\beta_2 = \arctan\frac{R_h}{x_h+\ell_h}$.

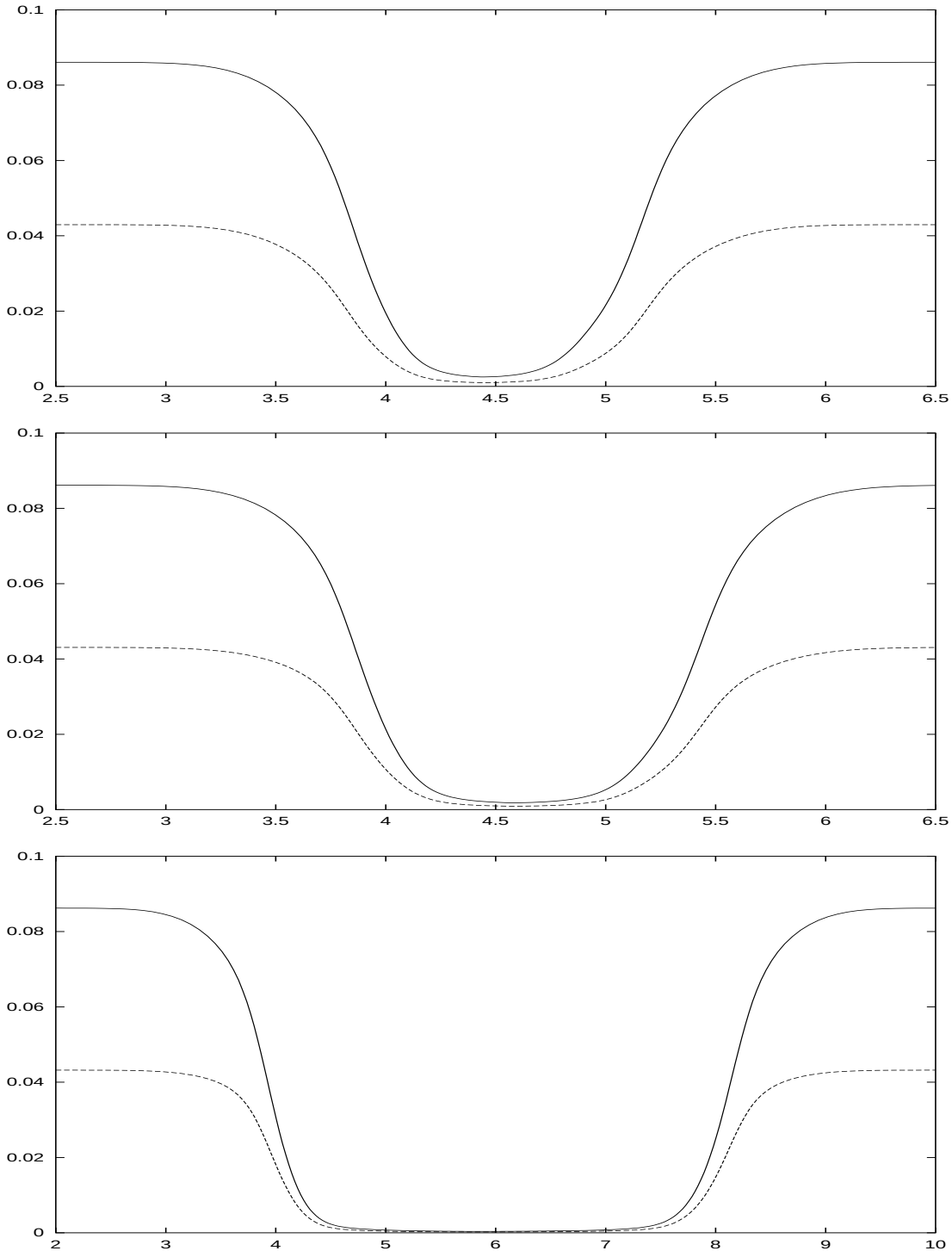

Figure 4: *Shape (outer (solid) and inner (dashed) radii) of glass tube when it breaks with θ_h^1=1500 K and θ_h^2=1100 K: $\beta_0 = 0.1$ (top); $\beta_0 = 0$ (middle); $\beta_0 = -0.1$ (bottom).*

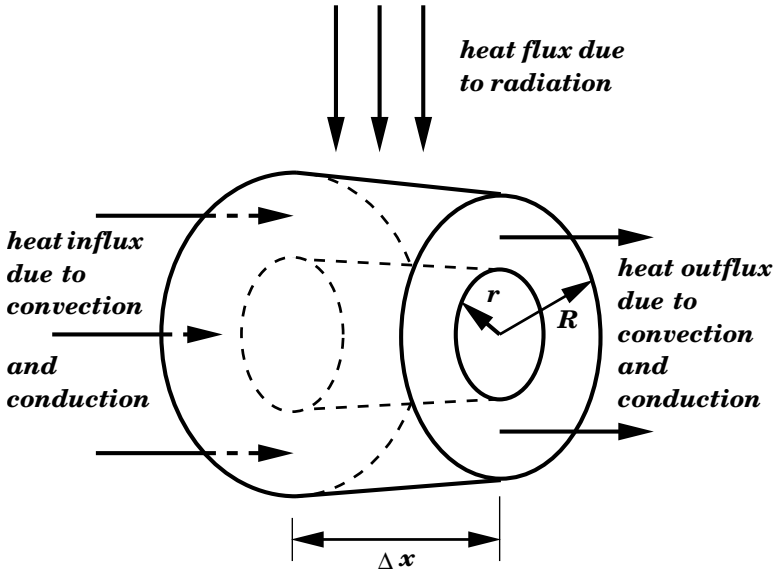

Figure 5: Schematic of the control volume for the conservation of energy in the glass tube.

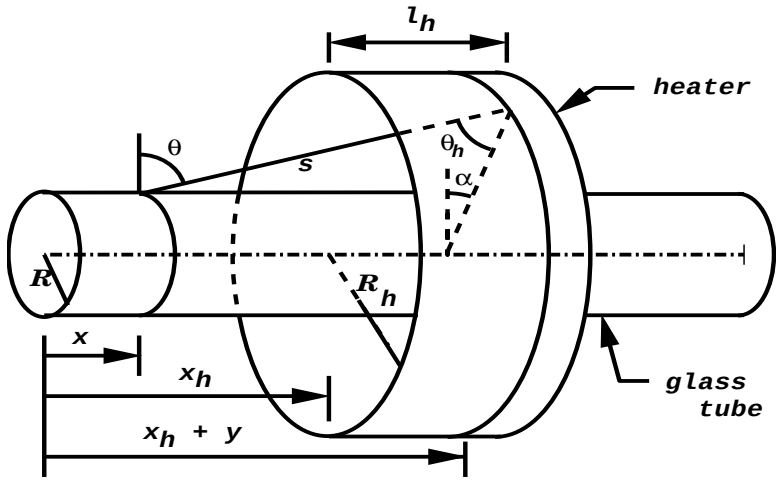

Figure 6: Geometry for radiative heat transfer from the heater to the glass tube.